Published in final edited form as:
Cell Transplant. 2008 ; 17(8): 911–922.

Assessment of a Nuclear Affinity Labeling Method for Tracking Implanted Mesenchymal Stem Cells

Merced Leiker, **Gen Suzuki**, **Vijay S. Iyer**, **John M. Canty Jr.**, and **Techung Lee**
Center for Research in Cardiovascular Medicine, University at Buffalo, Buffalo, NY, USA

Abstract

Therapeutic implantation of mesenchymal stem cells (MSCs) is entering the realm of clinical trials for several human diseases, and yet much remains uncertain regarding their dynamic distribution and cell fate after in vivo application. Discrepancies in the literature can be attributed in part to the use of different cell labeling/tracking methods and cell administration protocols. To identify a stem cell detection method suitable for myocardial implantation in a large animal model, we experimented on three different MSC labeling methods: adenovirus-mediated expression of enhanced green fluorescence protein (EGFP) and β-galactosidase (LacZ), and nuclear staining with DAPI. Intramuscular and intracoronary administrations of labeled porcine MSCs identified the nuclear affinity dye to be a reliable stem cell tracking marker. Stem cell identification is facilitated by an optimized live cell labeling condition generating bright blue fluorescence sharply confined to the nucleus. DAPI-labeled MSCs retained full viability, ceased proliferation, and exhibited an increased differentiation potential. The labeled MSCs remained fully active in expressing key growth factor and cytokine genes, and notably exhibited enhanced expression of the chemokine receptor CXCR4 and its ligand SDF1, indicating their competency in response to tissue injury. Histological analysis revealed that approximately half a million MSCs or ~2% of the administered MSCs remained localized in the normal pig heart 2 weeks after coronary infusion. That the vast majority of these identified MSCs were interstitial indicated the ability of MSCs to migrate across the coronary endothelium. No evidence was obtained indicating MSC differentiation to cardiomyocyte.

Keywords

Mesenchymal stem cells; Heart; Tracking; Implantation

INTRODUCTION

Stem cell therapy has in recent years received much attention in the field of regenerative medicine. Therapeutic implantation of mesenchymal stem cells (MSCs), in particular, has been attempted in several clinical trials for hematological disorders, cardiovascular diseases, osteogenesis imperfecta, neurological pathologies, and even cancer therapy (9,14,23). The ease of isolation, capacity for large-scale expansion, and alleged immunoprivileged status of MSCs (3,21,29) are likely to generate more clinical applications in the future. Central to these efforts is a thorough understanding of how MSCs achieve the observed therapeutic benefits and the fate of MSCs after implantation. It is believed that the multifaceted paracrine actions of MSCs explain at least in part their tissue-healing power (5,6,15,24). The

Address correspondence to Techung Lee, Department of Biochemistry, SUNY at Buffalo, 3435 Main Street, Buffalo, NY 14214, USA. Tel/fax: (716) 829-3106; chunglee@buffalo.edu.

extent to which stem cells engraft, integrate, and differentiate into different cell types after implantation in different settings is notably variable. Phenomena such as transdifferentiation, cell fusion, and intercellular communication through GAP junctions or nanotubes have been proposed to account for the seeming pluripotency of adult stem cells in various implantation studies (26,32,50,53,62). Technically, these discrepancies may be caused in part by the use of different cell labeling/tracking methods, cell administration protocols, timing of cell transplantation after tissue injury, and possibly misinterpretation of microscopy results (4).

Many cell labeling techniques have been used for tracking implanted stem cells in vivo. Fluorescent quantum dots and iridium nanoparticles are randomly internalized by cells during culturing (13,41). Membrane dyes such as PKH26 and DiI are incorporated into cell membrane lipids through hydrophobic interaction (6,45). The nucleoside analog bromodeoxyuridine (BrdU) can be incorporated into genomic DNA, allowing labeled cells to be detected by an antibody directed against BrdU (22). DNA binding dyes such as DAPI and Hoechst stains, which are structurally similar, are available for live cell labeling because they are membrane permeable (7). Overexpression of reporter genes represents another approach for cell labeling, and the genes can encode green fluorescent protein (GFP) and its derivatives, β-galactosidase, luciferase, or thymidine kinase (60). Among these reporter proteins, GFP is unique and easy to use in that it does not require an added substrate for signal emission, and thus has gained wide use in cell tracking studies. Although GFP is generally assumed to be biologically inert, many reports of GFP toxicity affecting either cell viability, development, or physiology have been documented (8,12,16,17,36). In particular, transgenic expression of GFP in the mouse heart has been found to cause dilated cardiomyopathy (18).

We previously demonstrated that FGF5 gene therapy to porcine hibernating myocardium improved cardiac function (48). In preparation for MSC therapeutic applications in porcine hibernating myocardium, we experimented with several different live cell labeling methods to identify the one suitable for myocardial stem cell tracking in the large animal model. The work described here identified the nuclear affinity dye DAPI to be a reliable marker for monitoring MSC distribution after myocardial implantation in pigs. Further data were presented regarding the effect of DAPI labeling on the function and phenotype of MSCs.

MATERIALS AND METHODS

MSC Culture

Porcine bone marrow-derived MSCs were cultured as previously described (56). In brief, MSCs were cultured in Advanced-DMEM (ADMEM; Invitrogen, Grand Island, NY, USA) supplemented with 4% fetal bovine serum (FBS), 2 mM GlutaMax, and 50 μg/ml gentamycin, and incubated in a humidified 5% CO_2 atmosphere at 37°C. MSC cultures used in this work received less than 5 passages.

Cell Labeling

A 10 mg/ml DAPI (4′,6′-diamidino-2-phenylindole) stock solution was prepared in dimethyl sulfoxide (DMSO), and stored at −20°C. Aliquots of the DAPI stock solution were added to culture medium at a final concentration of 20 μg/ml. Cells were maintained in the DAPI-containing medium for ~16 h, after which cells were thoroughly rinsed with Hank's balanced salt solution (HBSS) prior to trypsinization. For EGFP and β-galactosidase (LacZ) labeling, MSCs were infected with the recombinant adenovirus Ad-EGFP and Ad-LacZ as described previously (35), and cells were mildly fixed with a 2% paraformaldehyde (PFA) solution for 5 min at 4°C 2 days after infection. For X-gal (5-bromo-4-chloro-3-indolyl-β-D-

galactopyranoside) staining, PFA-fixed cells were incubated in a substrate solution (60 mM HEPES pH 7.4, 133 mM NaCl, 3 mM $MgCl_2$, 3 mM potassium ferricyanide, 3 mM potassium ferrocyanide, and 0.5 mg/ ml X-gal) at 37°C until blue color appeared.

MTT Cell Proliferation and Cytotoxicity Assays

MSCs were plated onto 24-well plates in triplicate (10^4 cells/well) in the growth medium. Protocols for MTT assays were as described previously (35). In brief, after the overnight DAPI labeling, cells were washed with HBSS twice, and refed with the growth medium. Culture medium was removed at the time points indicated and stored frozen for cell injury assays. Growth medium (0.3 ml) containing 0.25 mg/ml MTT was added to each aspirated well, and cells were incubated at 37°C for 20 min, following which the medium was replaced by 0.2 ml DMSO per well. MTT dye conversion was determined by measuring the $OD_{540\ nm}$ of the DMSO extracts using DMSO as blank. Cell injury as determined by lactate dehydrogenase activities in the culture medium was determined as described previously (34). Assays were initiated by mixing 20 µl of each collected medium sample with 50 µl Cell Injury Assay Solution (Biomedical Research Service, Buffalo, NY, USA) in a 96-well plate. The plate was incubated at 37°C for 30–60 min, following which the reaction was terminated by addition of 50 µl 5% acetic acid to each well. Lactate dehydrogenase activities in the medium were measured at $OD_{492\ nm}$. Data presented are means ± SEs. Some error bars were too small to appear on the graph. Student's *t*-tests were used for statistical analysis.

MSC Differentiation Assays

Alkaline phosphatase (ALP) and Alcian blue binding assays were as described previously (35). Recombinant human bone morphogenetic protein-7 (BMP7) was purchased from R&D Systems (Minneapolis, MN, USA). MSCs plated on 60-mm dishes were incubated with 0.1 µg/ml BMP7 in ADMEM +1% FBS for 2 weeks, following which cells were rinsed once with HBSS and lysed in a cell lysis solution (PBS supplemented with 0.1% Triton X-100). Lysates were clarified briefly by centrifugation and used for both assays. Protein concentrations and ALP activities of the lysates were determined by the BCA protein assay kit (Pierce Biotech, Rockford, IL, USA) and the ALP assay kit (Biomedical Research Service, Buffalo, NY, USA), respectively. ALP activities were expressed as optical density units at 412 nm per milligram proteins. For the dye binding assay, lysates were mixed with five volumes of 1% Alcian blue solution prepared in 0.1 N hydrochloric acid at room temperature for 1 h. Precipitates were harvested by a 1-min centrifugation in a microfuge and extracted with DMSO. Extracted dyes were measured by absorbance at 620 nm.

RNA Preparation and Quantitative Reverse Transcription-Polymerase Chain Reaction (qRT-PCR)

Cells were lysed with RLT buffer supplied with the Qiagen's RNeasy RNA isolation kit (Valencia, CA, USA), and RNA was isolated according to the manufacturer's instructions. qRT-PCR was performed as follows. One µg RNA was used for reverse transcription using Superscript III reverse transcriptase (Invitrogen, Carlsbad, CA, USA) according to the manufacturer's instructions. PCR primers were designed using MIT's Primer3 software. Each PCR amplification product was verified by agarose gel electrophoresis followed by DNA sequencing confirmation. Real-time PCR was performed using the MyIQ machine with the SYBR green kit (Bio-Rad, Hercules, CA, USA). Amplification conditions after an initial denaturation step for 3 min at 95°C were: 95°C denaturing temperature (10 s) and 55°C annealing and elongation temperature (30 s) for 45 cycles. Melting curve analysis was performed to check for a single amplicon. MyIQ analysis software was used for determining crossing points. Data were analyzed by the $2^{\Delta\Delta CT}$ method, and presented as percent gene expression compared to control cells. Glyceraldehyde-3-phosphate dehydrogenase

(GAPDH) was used as the reference gene for calculations. Primer sequences for porcine cDNAs were: GAPDH—TGCCCAGAACATC (5′) and GGATGACCTTGCC (3′); FGF2—GGAGTGTGTG CAAACCGTTA (5′) and TCGTTTCAGTGCCACA TACC (3′); VEGF—CTACCTCCACCATGCCAAGT (5′) and ACACAGGACGGCTTGAAGAT (3′); IL-6—TTCACCTCTCCGGACAAAAC (5′) and TCTGCCAG TACCTCCTTGCT (3′); MCP1—CACCAGCAGCAA GTGTCCTA (5′) and TCCAGGTGGCTTATGGAGTC (3′); TGF-β1—AAGCGGCAACCAAATCTATG (5′) and CACGTGCTGCTCCACTTTTA (3′); CXCR4—CAGCAAGGGTGTGAGTTTGA (5′) and TCCAAG GAAAGCGTAGAGGA (3′); SDF1—CCTTGCCGAT TCTTTGAGAG (5′) and CAATTTTGGGTCAATGCA CA (3′).

Intramuscular and Intracoronary MSC Implantation

All experimental procedures and protocols conformed to institutional guidelines for the care and use of animals in research. For mouse intramuscular cell implantation, approximately half a million labeled porcine MSCs suspended in 0.1 ml HBSS were administered via direct injection into the soleus and gastrocnemius muscles of each 3-month-old male C3H mouse. Control animals received the same volume of HBSS. Injected muscle was harvested 2 and 4 weeks after cell implantation, and tissue samples were prepared for histological analysis (see below). For intracoronary cell implantation in pig hearts, MSCs were expanded to ~30 million cells and labeled. Cells were suspended in 30 ml HBSS and kept on ice until implantation. Normal 3–4-month-old farm-raised pigs of mixed sex were anesthetized and handled as described previously (48). Pigs were sedated (Telazol; tiletamine 50 mg/ml and zolazepam 50 mg/ml/xylazine 100 mg/ml, 0.022 mg/kg, IM), intubated, and ventilated with a 0.5–2% isoflurane/oxygen mixture. Cells were administered in equally divided doses into the left anterior descending, circumflex, and right coronary arteries over a period of ~20 min. Pigs were terminated 2 weeks after MSC implantation, and heart tissue from the left anterior descending and right coronary arteries was excised and processed for histological analysis.

Tissue Preparation and In Situ Hybridization

Mice were euthanized by CO_2 narcosis, and immediately transcardially perfused with ice-cold 10% sucrose in PBS. Excised mouse muscle or pig heart tissues were immediately fixed in a freshly prepared PBS solution containing 2% PFA, 0.1% glutaraldehyde, and 20% sucrose at a rate of 1 h per 2-mm tissue depth. Fixed tissue fragments were soaked in 20% sucrose again at a rate of 1 h per 2-mm tissue depth as previously described (4). Tissues were then quickly frozen in OCT medium in an isopentane/dry ice slurry. Frozen tissue was cut to 10-μm sections, refixed in 2% PFA for 5 min at 4°C, and then washed with PBS containing 0.1% Triton X-100 before histological analysis. H&E staining was performed by University at Buffalo histology core facility. Tissue actin filaments were stained with TRITC- or FITC-conjugated phalloidin (Sigma, St. Louis, IL, USA) for 30 min at room temperature and washed with PBS containing 0.1% Triton X-100 before mounting in Slow-fade Gold mounting medium (Invitrogen, Carlsbad, CA, USA). Mounting medium containing DAPI or propidium iodide (Vector Laboratories, Burlingame, CA, USA) was used where indicated. Some tissue sections were stained with a vWF antibody (#PC313; Calbiochem, San Diego, CA, USA) at 1:100 dilution. Frozen sections were brought to room temperature (10 min), fixed in 2% paraformaldehyde in PBS for 5 min, then washed and permeablized in PBS with 0.1% Triton X-100 for 3 × x5 min. Sections were blocked with 2% horse serum in PBS with 0.1% Triton X-100 and washed for 2 × 5 min before incubation with primary antibody at room temperature for 1 h. Sections were washed 3 × 5 min before incubation with secondary antibody at room temperature for 1 h. Sections were washed 3 × 5 min and then allowed to air dry for 5 min before mounting in Slowfade Gold mounting medium. Stained tissue sections were digitally imaged using an epifluorescent microscope equipped with structured illumination system for confocal-like optical sectioning (Zeiss

Axioimager Z1 with Apotome). The 400× *z*-stack images were collected at 0.5-μm thick layers. Images were viewed using Axiovision LE Version 4.5 software. The 200× images were digitally collected using an epifluorescent microscope (Nikon Eclipse E600). Confocal images were obtained using Bio-Rad MRC 1024 confocal microscope.

RESULTS

Various results have been reported in the literature regarding the dynamic distribution and cell fate of implanted stem cells in part due to the use of different cell labeling and tracking methods. To identify a stem cell labeling method suitable for myocardial implantation in our large-animal model, we initially experimented on three different MSC labeling methods: adenovirus-mediated expression of enhanced green fluorescence protein (EGFP) and β-galactosidase (LacZ), and live cell DAPI nuclear staining. Porcine bone marrow-derived MSCs could be readily labeled by each of these markers in culture. Note that the EGFP-labeled MSCs exhibited prominent green fluorescent nuclei with some cytosolic green fluorescence (Fig. 1A). We also note that this pattern of strong nuclear emission of green fluorescence is not readily discernible in cells expressing higher levels of EGFP. DAPI can interact with both DNA and RNA, and thus can label the cytosolic as well as the nuclear compartments (20). Brief incubation of live cells with high concentrations of DAPI results in the labeling of both cytosolic and nuclear compartments that appear diffuse (49,57). The fuzzy image of these labeled cells can pose a problem for tracking cells in vivo. We found that overnight incubation of cultured MSCs with 10–20 μg/ml DAPI in the culture medium resulted in prominent blue nuclear fluorescence with virtually no cytosolic fluorescence (Fig. 1B). This clearly defined intensely blue nuclear staining is technically advantageous for cell tracking as illustrated below. LacZ-labeled MSCs were visualized after a mild cell fixation in 2% PFA and subsequent incubation with the chromogenic substrate X-gal, which caused dark blue precipitates in the cells (Fig. 1C). It should be mentioned that prolonged fixation time was found to destroy MSC-associated EGFP and LacZ signals. The DAPI signals, on the other hand, were not affected by over fixation.

Although MSCs could be efficiently labeled by these methods in culture, whether these labels could be reliably detected after in vivo implantation, particularly in a large-animal model, needs to be examined. Major considerations include label stability, diffusibility, potential toxicity, and tissue autofluorescence. These issues can be better addressed in small rodents initially. To facilitate the analysis, we first attempted direct intramuscular MSC injection in mice, which would allow us to more accurately harvest the muscle tissue harboring the injected MSCs. Approximately half a million labeled porcine MSCs were directly injected into the mouse soleus and gastrocnemius muscles. This xenotransplantation approach was implemented based on the many reports that MSCs are immune privileged, and can be used in allogeneic and xenogeneic transplantation settings (2,11,30,33,38). Indeed, we did not observe any sign of tissue inflammation throughout the period of the studies. Injected muscle was excised 2 and 4 weeks after MSC implantation and prepared by cryostat sectioning for histological analysis using the method largely described by Brazelton and Blau (4). In particular, care was taken during tissue processing to avoid potential inactivation of EGFP and β-galactosidase by overfixation as noted above.

Figure 2A illustrates an H&E-stained cryostat section from injected muscle showing numerous MSCs interspersed between muscle fibers. In spite of the fact that EGFP- and LacZ-labeled MSCs could be readily demonstrated in culture, we experienced difficulties reliably demonstrating these labeled MSCs from the mouse muscle tissue sections. Although some cell-associated green fluorescence was detected, it lacked the nuclear emission pattern illustrated in Figure 1A, and therefore was of dubious origin. In contrast with the uncertainty and ambiguity associated with the EGFP and LacZ reporters, many DAPI-labeled MSC

nuclei could be readily identified from the muscle sections. The tissue sections were counterstained with phalloidin-TRITC (Fig. 2B, staining actin filaments) or propidium iodide (Fig. 2C, staining total nuclei) to highlight the distribution of these blue MSC nuclei. Tissue sections were also stained with an antibody specific for von Willebrand factor (vWF), an endothelial cell marker. A 400× *z*-stack image of vWF antibody-stained sections revealed a capillary structure containing three consecutive MSC nuclei (Fig. 2D), indicating de novo capillary formation mediated by injected MSCs, and consistent with the reports that MSCs are capable of differentiating into endothelial cells in culture and in vivo (43,47). Figure 2D also revealed several MSC nuclei apparently integrated into the muscle cells but positioned peripherally (indicated by arrows). These integrated MSC nuclei were pressed against sarcolemma, becoming elliptical in shape. Because newly generated muscle cells typically exhibit centrally positioned nuclei, these peripherally positioned blue fluorescent nuclei indicated MSC fusion with the existing muscle fiber.

Our difficulties in detecting specific EGFP and LacZ signals from tissue sections could stem from the observation that these reporter proteins become highly diffusible when tissue sections are only mildly fixed in order to preserve reporter protein activity as elaborated by Brazelton and Blau (4). However, because tissue over-fixation can destroy EGFP and LacZ signals, finding EGFP- or LacZ-marked stem cells from injected tissue can be problematic. Further, leaky EGFP and LacZ reporter proteins can lead to misidentification of injected stem cells. These considerations prompted us to adopt the DAPI labeling method for our porcine myocardial MSC transplantation work (see below).

Although DAPI has been used by other stem cell researchers for cell tracking in vivo (7,57), it remains unknown whether this compound may alter the function or phenotype of the labeled stem cells. This question is particularly relevant because DAPI through interacting with genomic DNA may differentially affect gene expression as observed with some DNA-modifying compounds such as 5-azacytidine or bromodeoxyuridine (28,31). We examined MSC growth kinetics after DAPI labeling or treatment with the vehicle DMSO. MTT cell proliferation assays shown in Figure 3 reveal that DAPI inhibited the proliferation potential of MSCs. In spite of the growth-inhibitory effect of DAPI, the labeled MSCs remained viable because they were morphologically indistinguishable from unlabeled MSCs. This was further substantiated by a sensitive cytotoxicity assay based on the release of the cytosolic enzyme lactate dehydrogenase into the culture medium (25), which showed that cell membrane integrity was not compromised by DAPI labeling (Fig. 4). Because an inverse correlation usually exists between cell proliferation and differentiation, we next examined whether the differentiation potential of MSCs might be affected by DAPI labeling. DMSO- and DAPI-treated MSCs were exposed to BMP7 to induce osteochondrogenic differentiation (35). As expected, BMP7 promoted MSC osteochondrogenic differentiation as indicated by increased alkaline phosphatase and Alcian blue binding activities (Fig. 5). Notably, DAPI-labeled MSCs exhibited a fourfold increase in alkaline phosphatase activities (left panel), suggesting that the osteogenic potential was enhanced by DAPI. However, the chondrogenic potential of MSCs was not significantly affected by DAPI (right panel). Thus, DAPI labeling differentially affects the differentiation potential of MSCs.

Although MSCs possess multilineage potentials, the cardiac therapeutic effects of MSCs are now thought to be largely mediated by their paracrine actions (i.e., their abilities to produce a multitude of growth factors and cytokines) (5,6,15,24). It is therefore critical to determine whether DAPI labeling may adversely affect the paracrine actions of MSCs. qRT-PCR was performed to examine the expression of several growth factor and cytokine genes. Fibroblast growth factor (FGF) and vascular endothelial growth factor (VEGF) in particular are well known for their regulatory and therapeutic effects on the cardiovascular system (48,58). The CXCR4– SDF1 chemokine axis was also included in the analysis due to their involvement

in stem cell homing (19,59,61). Figure 6 shows that expression of FGF2, VEGF, interleukin-6 (IL-6), monocyte chemotactic protein-1 (MCP1), and transforming growth factor-β1 (TGF-β1) were not significantly affected by DAPI labeling. Intriguingly, expression of CXCR4 and its ligand SDF1 were each upregulated approximately twofold by DAPI labeling. These results thus indicate that expression of key growth factor and cytokine genes were not affected by DAPI labeling, and that the homing potential of MSCs in response to tissue injury may be enhanced by DAPI labeling.

We previously demonstrated that FGF5 gene therapy to porcine hibernating myocardium improved cardiac function (48). Having characterized and validated the DAPI labeling method, we next evaluated whether the DAPI labeling strategy might be consistently and reliably used for myocardial MSC tracking in the large-animal model. The first consideration was how to administer MSCs to the porcine heart. Although direct intramyocardial injection can allow us to localize administered MSCs with more precision and have a higher cell retention rate (52), this approach is quite invasive, often clinically unsuitable, and can introduce harmful scar tissue or cause arrhythmia in the heart (10). Systemic intravenous delivery of MSCs, although an attractive approach, has been shown to cause entrapment of MSCs in the lungs (1). Intracoronary delivery is the preferred route for global myocardial diseases such as heart failure and cardiomyopathy (40). Approximately 30 million MSCs per pig were labeled with DAPI and administered to the heart through intracoronary infusion. Heart tissues from the left anterior descending and right coronary arteries were excised for histological analysis 2 weeks after implantation. The 400× *z*-stack images of phalloidin-stained heart sections reveal predominantly interstitial DAPI-labeled MSC nuclei (Fig. 7A, cross section and Fig. 7B, longitudinal section). These interstitial MSCs could be detected with a frequency of approximately one MSC per 1 × 1 cm 10-μm tissue section on average (or ~1,000 MSCs per cm^3 heart tissue), indicating the ability of MSCs to migrate across the coronary endothelium. This observation implies that approximately half a million MSCs or ~2% of the infused MSCs remained localized in the pig heart 2 weeks after coronary infusion. Much less frequently detected were MSC nuclei positioned in line with resident endothelial nuclei (stained with propidium iodide) along the illustrated capillary (Fig. 7C). We did not detect any MSC nucleus associated with cardiac muscle fiber, consistent with the notion that MSCs do not readily become cardiomyocytes after implantation (39,47). Pigs were also implanted with EGFP-labeled MSCs through intracoronary infusion. However, we were again unable to detect convincing MSC-derived EGFP signals (data not shown).

DISCUSSION

Reliable stem cell labeling in vitro and cell tracking in vivo after implantation continue to pose a technical challenge. In practice, labels such as DiI and tagged nanoparticles (such as Quantum dots) generate fluorescent speckles in the labeled cells that lack structural hall-mark, and these dotted signals are often difficult to identify with certainty after in vivo cell implantation. Previous reports based on DiI labeling claiming MSC differentiation into cardiomyocytes should therefore be interpreted with caution (6,46). Also not well recognized in the field is that the use of reporter proteins such as EGFP and LacZ can be confounded by label stability, diffusibility, potential toxicity, and tissue autofluorescence. Indeed, we experienced inconsistency attempting to track EGFP- and LacZ-labeled MSCs. Our results show that the DAPI label can be stably retained in the implanted MSCs for at least 1 month after implantation, and these labeled MSCs can be detected histologically with little ambiguity. This is mainly due to the brightly and uniformly emitted blue fluorescence that is well confined to the nucleus and the low wavelength range used for signal detection (358 nm for excitation and 461 nm for emission).

DAPI is known to interact with AT clusters in the minor groove of double-stranded DNA (27), and this property of DAPI may be expected to have some selective effects on gene expression. Indeed, we show that DAPI can exert reciprocal effects on MSC proliferation and differentiation without affecting cell viability. Although MSC proliferation is inhibited by DAPI, trophic activities of MSCs remain intact as assessed by qRT-PCR. This conclusion is substantiated by the finding that DAPI stimulates the expression of the CXCR4–SDF1 axis. The finding is intriguing given the apparent importance of stem cell homing in tissue repair. In particular, the interaction between CXCR4 and SDF1 has been shown to mediate the migration of MSCs to damaged tissue sites (19,37). Our qRT-PCR analysis indicates that DAPI labeling does not interfere with the homing ability of MSCs.

At least five mechanisms are proposed to account for the cardiovascular beneficial effects of MSCs in various animal models. First, differentiation of administered MSCs into the cellular constituents of the heart can improve flow and function. Although our studies of myocardial MSC implantation indicate that MSCs do not readily differentiate into cardiomyocytes after pig heart implantation, MSC differentiation into endothelial cells in vitro and enhancing vascular density in several cardiomyopathy models have been demonstrated (7,24,49). In this aspect, the cardiovascular effect of MSCs mimics that mediated by VEGF. Second, MSCs can release trophic factors mediating paracrine actions (5,6,15,24,44). This mechanism explains why cardiovascular benefits of MSCs can be demonstrated even in the presence of low myocardial MSC engraftment after cell administration. This notion is consistent with the demonstration that MSC transplantation using cell sheet technology repairs scarred myocardium, indicating that MSCs need not be infused or injected to exhibit their beneficial effects (42). We have found that even at a ~2% engraftment efficiency MSCs after intracoronary infusion into porcine hibernating myocardium improved cardiac function significantly and that the DAPI-labeled MSCs retained their therapeutic potency (manuscript in preparation). These findings are consistent with the demonstration here that expression of growth factor and cytokine genes was not adversely affected by DAPI labeling. Third, fusion of administered MSCs with the resident constituents of the heart also helps retain MSCs. This mechanism appears to be more prevalent with the intramuscular injection approach, as shown in Figure 2. Fourth, stimulation of endogenous repair by injected MSCs may prove to be a potent mechanism for cardiac regeneration. Because studies have shown that endogenous cardiac stem cells can be stimulated via paracrine effects to reduce postinfarct remodeling (55), the paracrine actions of the interstitially localized MSCs may play a critical role in reviving cardiac stem cells for tissue repair and regeneration. Lastly, the anti-inflammatory function of MSCs may be particularly relevant in managing inflammatory cardiomyopathic conditions (51,54). This unique property of MSCs may have contributed to the success of the MSC xenotransplantation approach used here, allowing us to detect DAPI-labeled MSCs 1 month after cell implantation.

In summary, we presented results showing that the DAPI labeling strategy could be reliably used for MSC tracking in both small- and large-animal models. The brightly emitted blue fluorescence is exclusively confined to the nucleus, generating a sharp nuclear image advantageous for stem cell identification. Because MSCs cease proliferation after DAPI labeling, the DAPI signals are stably and uniformly retained in the cells for at least 1 month after cell implantation. This stem cell tracking strategy allows us to obtain the estimate that approximately 2% of the administered MSCs engraft in the interstitial space of the normal pig heart after intra-coronary infusion.

Acknowledgments

The work was supported by NIH grants HL55324, HL61610, and HL84590.

REFERENCES

1. Barbash IM, Chouraqui P, Baron J, Feinberg MS, Etzion S, Tessone A, Miller L, Guetta E, Zipori D, Kedes LH, Kloner RA, Leor J. Systemic delivery of bone marrow-derived mesenchymal stem cells to the infarcted myocardium: Feasibility, cell migration, and body distribution. Circulation 2003;108:863–868. [PubMed: 12900340]
2. Bartholomew A, Patil S, Mackay A, Nelson M, Buyaner D, Hardy W, Mosca J, Sturgeon C, Siatskas M, Mahmud N, Ferrer K, Deans R, Moseley A, Hoffman R, Devine SM. Baboon mesenchymal stem cells can be genetically modified to secrete human erythropoietin in vivo. Hum. Gene Ther 2001;12:1527–1541. [PubMed: 11506695]
3. Beggs KJ, Lyubimov A, Borneman JN, Bartholomew A, Moseley A, Dodds R, Archambault MP, Smith AK, McIntosh KR. Immunologic consequences of multiple, high-dose administration of allogeneic mesenchymal stem cells to baboons. Cell Transplant 2006;15:711–721. [PubMed: 17269442]
4. Brazelton TR, Blau HM. Optimizing techniques for tracking transplanted stem cells in vivo. Stem Cells 2005;23:1251–1265. [PubMed: 16109764]
5. Caplan AI, Dennis JE. Mesenchymal stem cells as trophic mediators. J. Cell. Biochem 2006;98:1076–1084. [PubMed: 16619257]
6. Dai W, Hale SL, Martin BJ, Kuang JQ, Dow JS, Wold LE, Kloner RA. Allogeneic mesenchymal stem cell transplantation in postinfarcted rat myocardium: Short- and long-term effects. Circulation 2005;112:214–223. [PubMed: 15998673]
7. Davani S, Marandin A, Mersin N, Royer B, Kantelip B, Herve P, Etievent JP, Kantelip JP. Mesenchymal progenitor cells differentiate into an endothelial phenotype, enhance vascular density, and improve heart function in a rat cellular cardiomyoplasty model. Circulation 2003;108:II253–II258. [PubMed: 12970242]
8. Detrait ER, Bowers WJ, Halterman MW, Giuli-ano RE, Bennice L, Federoff HJ, Richfield EK. Reporter gene transfer induces apoptosis in primary cortical neurons. Mol. Ther 2002;5:723–730. [PubMed: 12027556]
9. Devine SM. Mesenchymal stem cells: Will they have a role in the clinic? J. Cell. Biochem 2002;38:73–79.
10. Dhein S, Garbade J, Rouabah D, Abraham G, Ungemach FR, Schneider K, Ullmann C, Aupperle H, Gummert JF, Mohr FW. Effects of autologous bone marrow stem cell transplantation on beta-adrenoceptor density and electrical activation pattern in a rabbit model of non-ischemic heart failure. J. Cardiothorac. Surg 2006;1:17. [PubMed: 16800896]
11. Djouad F, Plence P, Bony C, Tropel P, Apparailly F, Sany J, Noel D, Jorgensen C. Immunosuppressive effect of mesenchymal stem cells favors tumor growth in allogeneic animals. Blood 2003;102:3837–3844. [PubMed: 12881305]
12. Endemann G, Schechtman D, Mochly-Rosen D. Cytotoxicity of pEGFP vector is due to residues encoded by multiple cloning site. Anal. Biochem 2003;313:345–347. [PubMed: 12605876]
13. Freyman T, Polin G, Osman H, Crary J, Lu M, Cheng L, Palasis M, Wilensky RL. Aquantitative randomized study evaluating three methods of mesenchymal stem cell delivery following myocardial infarction. Eur. Heart J 2006;27:1114–1122. [PubMed: 16510464]
14. Giordano A, Galderisi U, Marino IR. From the laboratory bench to the patient's bedside: An update on clinical trials with mesenchymal stem cells. J. Cell Physiol 2007;211:27–35. [PubMed: 17226788]
15. Gnecchi M, He H, Noiseux N, Liang OD, Zhang L, Morello F, Mu H, Melo LG, Pratt RE, Ingwall JS, Dzau VJ. Evidence supporting paracrine hypothesis for Akt-modified mesenchymal stem cell-mediated cardiac protection and functional improvement. FASEB J 2006;20:661–669. [PubMed: 16581974]
16. Hanazono Y, Terao K, Shibata H, Nagashima T, Ageyama N, Asano T, Ueda Y, Kato I, Kume A, Hasegawa M, Ozawa K. Introduction of the green fluorescent protein gene into hematopoietic stem cells results in prolonged discrepancy of in vivo transduction levels between bone marrow progenitors and peripheral blood cells in nonhuman primates. J. Gene Med 2002;4:470–477. [PubMed: 12221639]

17. Hanazono Y, Yu JM, Dunbar CE, Emmons RV. Green fluorescent protein retroviral vectors: Low titer high recombination frequency suggest a selective disadvantage. Hum. Gene Ther 1997;8:1313–1319. [PubMed: 9295126]

18. Huang W-Y, Aramburu J, Douglas PS, Izumo S. Transgenic expression of green fluorescence protein can cause dilated cardiomyopathy. Nat. Med 2000;6:482–483. [PubMed: 10802676]

19. Ji JF, He BP, Dheen ST, Tay SS. Interactions of chemokines and chemokine receptors mediate the migration of mesenchymal stem cells to the impaired site in the brain after hypoglossal nerve injury. Stem Cells 2004;22:415–427. [PubMed: 15153618]

20. Kapuscinski J. Interactions of nucleic acids with fluorescent dyes: Spectral properties of condensed complexes. J. Histochem. Cytochem 1990;38:1323–1329. [PubMed: 1696951]

21. Keyser KA, Beagles KE, Kiem HP. Comparison of mesenchymal stem cells from different tissues to suppress T-cell activation. Cell Transplant 2007;16:555–562. [PubMed: 17708345]

22. Kicic A, Shen WY, Wilson AS, Constable IJ, Robertson T, Rakoczy PE. Differentiation of marrow stromal cells into photoreceptors in the rat eye. J. Neurosci 2003;23:7742–7749. [PubMed: 12944502]

23. Kim BG, Hwang DH, Lee SI, Kim EJ, Kim SU. Stem cell-based cell therapy for spinal cord injury. Cell Transplant 2007;16:355–364. [PubMed: 17658126]

24. Kinnaird T, Stabile E, Burnett MS, Lee CW, Barr S, Fuchs S, Epstein SE. Marrow-derived stromal cells express genes encoding a broad spectrum of arteriogenic cytokines promote in vitro in vivo arteriogenesis through paracrine mechanisms. Circ. Res 2004;94:678–685. [PubMed: 14739163]

25. Korzeniewski C, Callewaert DM. An enzyme-release assay for natural cytotoxicity. J. Immunol. Methods 1983;64:313–320. [PubMed: 6199426]

26. Koyanagi M, Brandes RP, Haendeler J, Zeiher AM, Dimmeler S. Cell-to-cell connection of endothelial progenitor cells with cardiac myocytes by nanotubes: A novel mechanism for cell fate changes? Circ. Res 2005;96:1–4.

27. Kubista M, Akerman B, Norden B. Characterization of interaction between DNA and 4′,6-diamidino-2-phenylindole by optical spectroscopy. Biochemistry 1987;26:4545–4553. [PubMed: 3663606]

28. Lassar AB, Paterson BM, Weintraub H. Transfection of a DNA locus that mediates the conversion of 10T1/ 2 fibroblasts to myoblasts. Cell 1986;47:649–656. [PubMed: 2430720]

29. Le Blanc K, Pittenger M. Mesenchymal stem cells: Progress toward promise. Cytotherapy 2005;7:36–45. [PubMed: 16040382]

30. Le Blanc K, Tammik C, Rosendahl K, Zetterberg E, Ringden O. HLA expression immunologic properties of differentiated undifferentiated mesenchymal stem cells. Exp. Hematol 2003;31:890–896. [PubMed: 14550804]

31. Lee T, Shi Y, Schwartz RJ. Displacement of BrdUrd-induced YY1 by serum response factor activates skeletal a-actin transcription in embryonic myoblasts. Proc. Natl. Acad. Sci. USA 1992;89:9814–9818. [PubMed: 1409704]

32. Liang L, Bickenbach JR. Somatic epidermal stem cells can produce multiple cell lineages during development. Stem Cells 2002;20:21–31. [PubMed: 11796919]

33. Liechty KW, MacKenzie TC, Shaaban AF, Radu A, Moseley AM, Deans R, Marshak DR, Flake AW. Human mesenchymal stem cells engraft, demonstrate site-specific differentiation after in utero transplantation in sheep. Nat. Med 2000;6:1282–1286. [PubMed: 11062543]

34. Lin H, McGrath J, Wang P, Lee T. Cellular toxicity induced by SRF-mediated transcriptional squelching. Toxicol. Sci 2007;96:83–91. [PubMed: 17116645]

35. Lin H, Shabbir A, Molnar M, Lee T. Stem cell regulatory function mediated by expression of a novel mouse Oct4 pseudogene. Biochem. Biophys. Res. Commun 2007;355:111–116. [PubMed: 17280643]

36. Liu HS, Jan MS, Chou CK, Chen PH, Ke NJ. Is green fluorescent protein toxic to the living cells? Biochem. Biophys. Res. Commun 1999;260:712–717. [PubMed: 10403831]

37. Ma J, Ge J, Zhang S, Sun A, Shen J, Chen L, Wang K, Zou Y. Time course of myocardial stromal cell-derived factor 1 expression, beneficial effects of intravenously administered bone marrow stem cells in rats with experimental myocardial infarction. Basic Res. Cardiol 2005;100:217–223. [PubMed: 15754085]

38. Mansilla E, Marin GH, Sturla F, Drago HE, Gil MA, Salas E, Gardiner MC, Piccinelli G, Bossi S, Salas E, Petrelli L, Iorio G, Ramos CA, Soratti C. Human mesenchymal stem cells are tolerized by mice and improve skin and spinal cord injuries. Transplant. Proc 2005;37:292–294. [PubMed: 15808623]
39. Mazhari R, Hare JM. Advances in cell-based therapy for structural heart disease. Prog. Cardiovas. Dis 2007;49:387–395.
40. Melo LG, Pachori AS, Kong D, Gnecchi M, Wang K, Pratt RE, Dzau VJ. Gene and cell-based therapies for heart disease. FASEB J 2004;18:648–663. [PubMed: 15054087]
41. Michalet X, Pinaud FF, Bentolila LA, Tsay JM, Doose S, Li JJ, Sundaresan G, Wu AM, Gambhir SS, Weiss S. Quantum dots for live cells, in vivo imaging, and diagnostics. Science 2005;307:538–544. [PubMed: 15681376]
42. Miyahara Y, Nagaya N, Kataoka M, Yanagawa B, Tanaka K, Hao H, Ishino K, Ishida H, Shimizu T, Kangawa K, Sano S, Okano T, Kitamura S, Mori H. Monolayered mesenchymal stem cells repair scarred myocardium after myocardial infarction. Nat. Med 2006;12:459–465. [PubMed: 16582917]
43. Oswald J, Boxberger S, Jorgensen B, Feldmann S, Ehninger G, Bornhauser M, Werner C. Mesenchymal stem cells can be differentiated into endothelial cells in vitro. Stem Cells 2004;22:377–384. [PubMed: 15153614]
44. Pisati F, Bossolasco P, Meregalli M, Cova L, Belicchi M, Gavina M, Marchesi C, Calzarossa C, Soligo D, Lambertenghi-Deliliers G, Bresolin N, Silani V, Torrente Y, Polli E. Induction of neurotrophin expression via human adult mesenchymal stem cells: Implication for cell therapy in neurodegenerative diseases. Cell Transplant 2007;16:41–55. [PubMed: 17436854]
45. Sanchez-Ramos J, Song S, Dailey M, Cardozo-Pelaez F, Hazzi C, Stedeford T, Willing A, Freeman TB, Saporta S, Zigova T, Sanberg PR, Snyder EY. The X-gal caution in neural transplantation studies. Cell Transplant 2000;9:657–667. [PubMed: 11144962]
46. Shake JG, Gruber PG, Baumgartner WA, Senechal G, Meyers J, Redmond JM, Pittenger MF, Martin BJ. Mesenchymal stem cell implantation in a swine myocardial infarct model: Engraftment functional effects. Ann. Thorac. Surg 2002;73:1919–1926. [PubMed: 12078791]
47. Silva GV, Litovsky S, Assad JA, Sousa AL, Martin BJ, Vela D, Coulter SC, Lin J, Ober J, Vaughn WK, Branco RV, Oliveira EM, He R, Geng YJ, Willerson JT, Perin EC. Mesenchymal stem cells differentiate into an endothelial phenotype, enhance vascular density, and improve heart function in a canine chronic ischemia model. Circulation 2005;111:150–156. [PubMed: 15642764]
48. Suzuki G, Lee T, Fallavollita JA, Canty JM Jr. Adenoviral gene transfer of FGF-5 to hibernating myocardium improves function stimulates myocytes to hypertrophy and reenter the cell cycle. Circ. Res 2005;96:767–775. [PubMed: 15761196]
49. Tang J, Xie Q, Pan G, Wang J, Wang M. Mesenchymal stem cells participate in angiogenesis and improve heart function in rat model of myocardial ischemia with reperfusion. Eur. J. Cardiothorac. Surg 2006;30:353–361. [PubMed: 16829080]
50. Terada N, Hamazaki T, Oka M, Hoki M, Mastalerz DM, Nakano Y, Meyer EM, Morel L, Petersen BE, Scott EW. Bone marrow cells adopt the phenotype of other cells by spontaneous cell fusion. Nature 2002;416:542–545. [PubMed: 11932747]
51. Togel F, Hu Z, Weiss K, Isaac J, Lange C, Westen-felder C. Administered mesenchymal stem cells protect against ischemic acute renal failure through differentiation-independent mechanisms. Am. J. Physiol. Renal. Physiol 2005;289:F31–F42. [PubMed: 15713913]
52. Tran N, Li Y, Maskali F, Antunes L, Maureira P, Laurens MH, Marie PY, Karcher G, Groubatch F, Stoltz JF, Villemot JP. Short-term heart retention and distribution of intramyocardial delivered mesenchymal cells within necrotic or intact myocardium. Cell Transplant 2006;15:351–358. [PubMed: 16898229]
53. Tsai RYL, Kittappa R, McKay RDG. Plasticity, niches, and the use of stem cells. Dev. Cell 2002;2:707–712. [PubMed: 12062083]
54. Uccelli A, Pistoia V, Moretta L. Mesenchymal stem cells: a new strategy for immunosuppression? Trends Immunol 2007;28:219–226. [PubMed: 17400510]
55. Urbanek K, Rota M, Cascapera S, Bearzi C, Nascimbene A, De Angelis A, Hosoda T, Chimenti S, Baker M, Limana F, Nurzynska D, Torella D, Rotatori F, Rastaldo R, Musso E, Quaini F, Leri A,

Kajstura J, Anversa P. Cardiac stem cells possess growth factor-receptor systems that after activation regenerate the infarcted myocardium, improving ventricular function long-term survival. Circ. Res 2005;97:663–673. [PubMed: 16141414]

56. Vacanti V, Kong E, Suzuki G, Sato K, Canty JM Jr, Lee T. Phenotypic changes of adult porcine mesenchymal stem cells induced by prolonged passaging in culture. J. Cell Physiol 2005;205:194–201. [PubMed: 15880640]
57. Wang JS, Shum-Tim D, Galipeau J, Chedrawy E, Eliopoulos N, Chiu RC. Marrow stromal cells for cellular cardiomyoplasty: Feasibility potential clinical advantages. J. Thorac. Cardiovasc. Surg 2000;120:999–1005. [PubMed: 11044327]
58. Wang X, Hu Q, Mansoor A, Lee J, Wang Z, Lee T, From AH, Zhang J. Bioenergetic and functional consequences of stem cell-based VEGF delivery in pressure-overloaded swine hearts. Am. J. Physiol. Heart Circ. Physiol 2006;290:H1393–H1405. [PubMed: 16387794]
59. Wynn RF, Hart CA, Corradi-Perini C, O'Neill L, Evans CA, Wraith JE, Fairbairn LJ, Bellantuono I. A small proportion of mesenchymal stem cells strongly expresses functionally active CXCR4 receptor capable of promoting migration to bone marrow. Blood 2004;104:2643–2645. [PubMed: 15251986]
60. Yaghoubi SS, Barrio JR, Namavari M, Satyamurthy N, Phelps ME, Herschman HR, Gambhir SS. Imaging progress of herpes simplex virus type 1 thymidine kinase suicide gene therapy in living subjects with positron emission tomography. Cancer Gene Ther 2005;12:329–339. [PubMed: 15592447]
61. Yamaguchi J, Kusano KF, Masuo O, Kawamoto A, Silver M, Murasawa S, Bosch-Marce M, Masuda H, Losordo DW, Isner JM, Asahara T. Stromal cell-derived factor-1 effects on ex vivo expanded endothelial progenitor cell recruitment for ischemic neovascularization. Circulation 2003;107:1322–1328. [PubMed: 12628955]
62. Ying Q-L, Nichols J, Evans EP, Smith AG. Changing potency by spontaneous fusion. Nature 2002;416:545–548. [PubMed: 11932748]

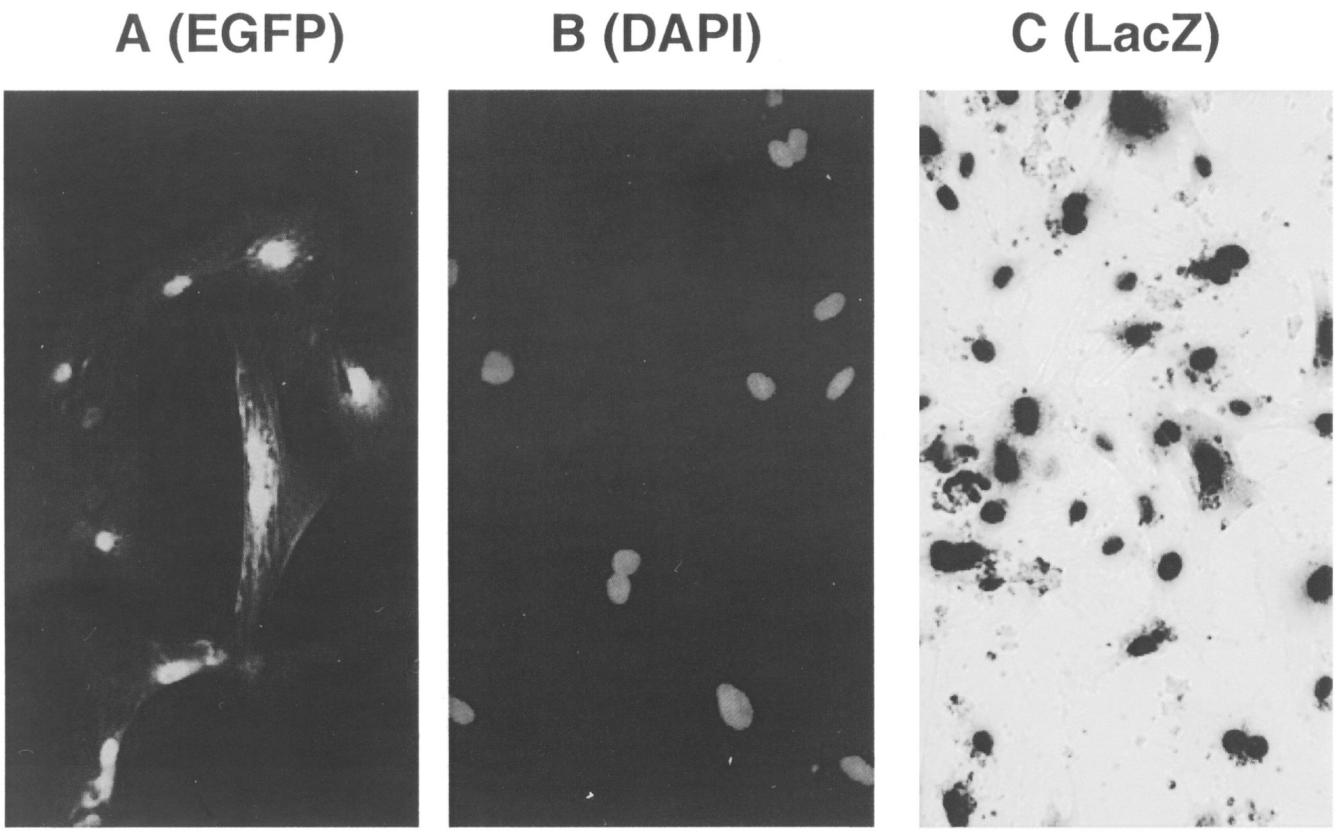

Figure 1.
Fluorescent and colorimetric labeling of MSCs in culture. Porcine MSCs plated and grown on coverslips were infected with recombinant adenovirus expressing EGFP (A) and β-galactosidase (C). MSCs were incubated with 20 μg/ml DAPI in culture medium overnight (B). All images were acquired digitally (200×) using an epifluorescent microscope (Nikon Eclipse E600).

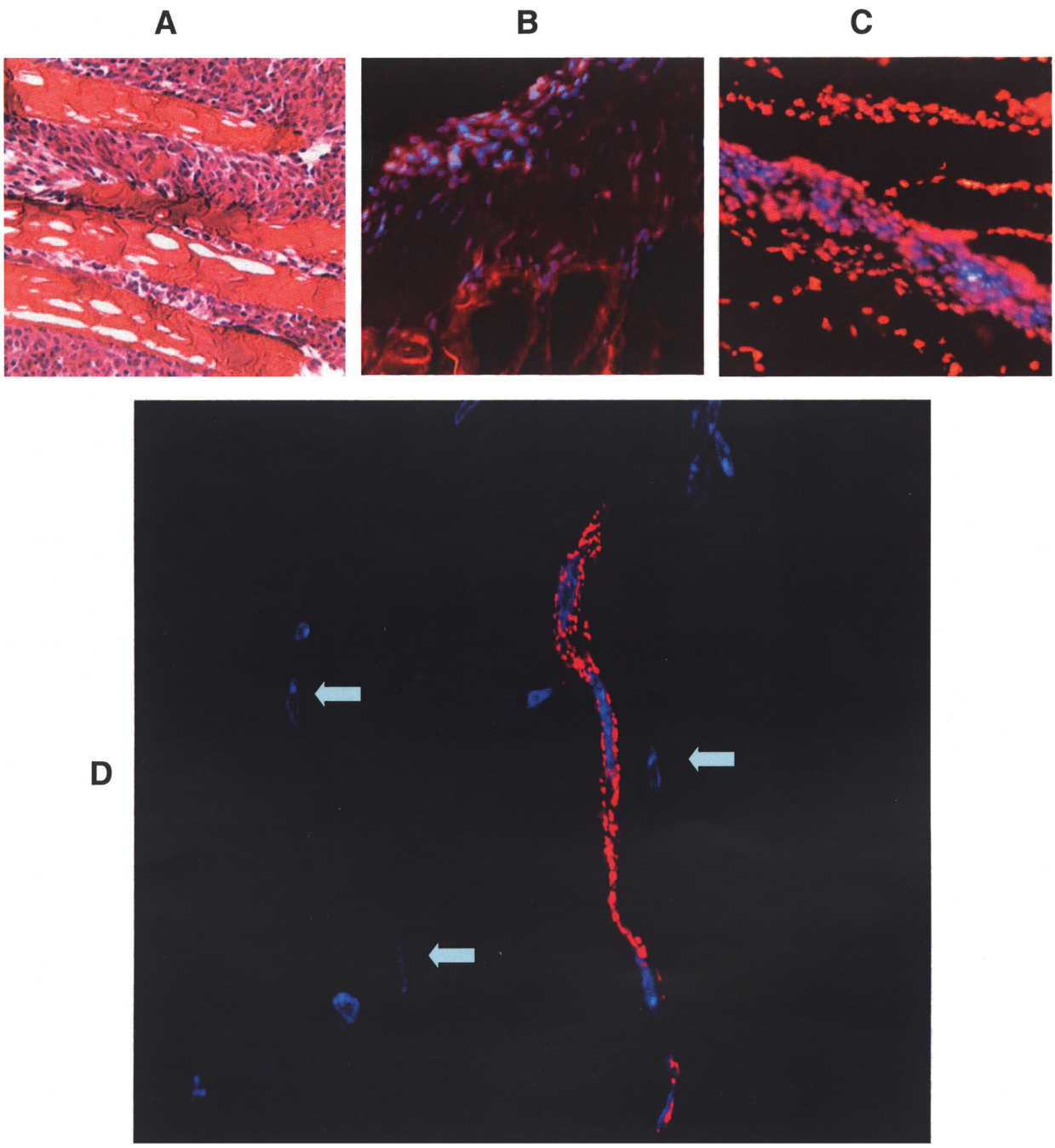

Figure 2.

Mouse skeletal muscle sections showing the distribution of intramuscularly injected DAPI-labeled MSCs. Muscle tissue 2 or 4 weeks after cell implantation were prepared by cryostat sectioning and stained by H&E (A). Tissue sections were counter-stained with TRITC-conjugated phalloidin (B) or with propidium iodide (C). Images shown in (A) to (C) were acquired digitally (200×) using an epifluorescent microscope (Nikon Eclipse E600). Tissue sections were stained with a vWF antibody to reveal capillary structures (D). The 400× *z*-stack image was obtained using an epifluorescent microscope Zeiss Axioimager Z1 with Apotome. The image background reveals the contour of muscle cells, highlighting three integrated MSC nuclei, which are indicated by arrows.

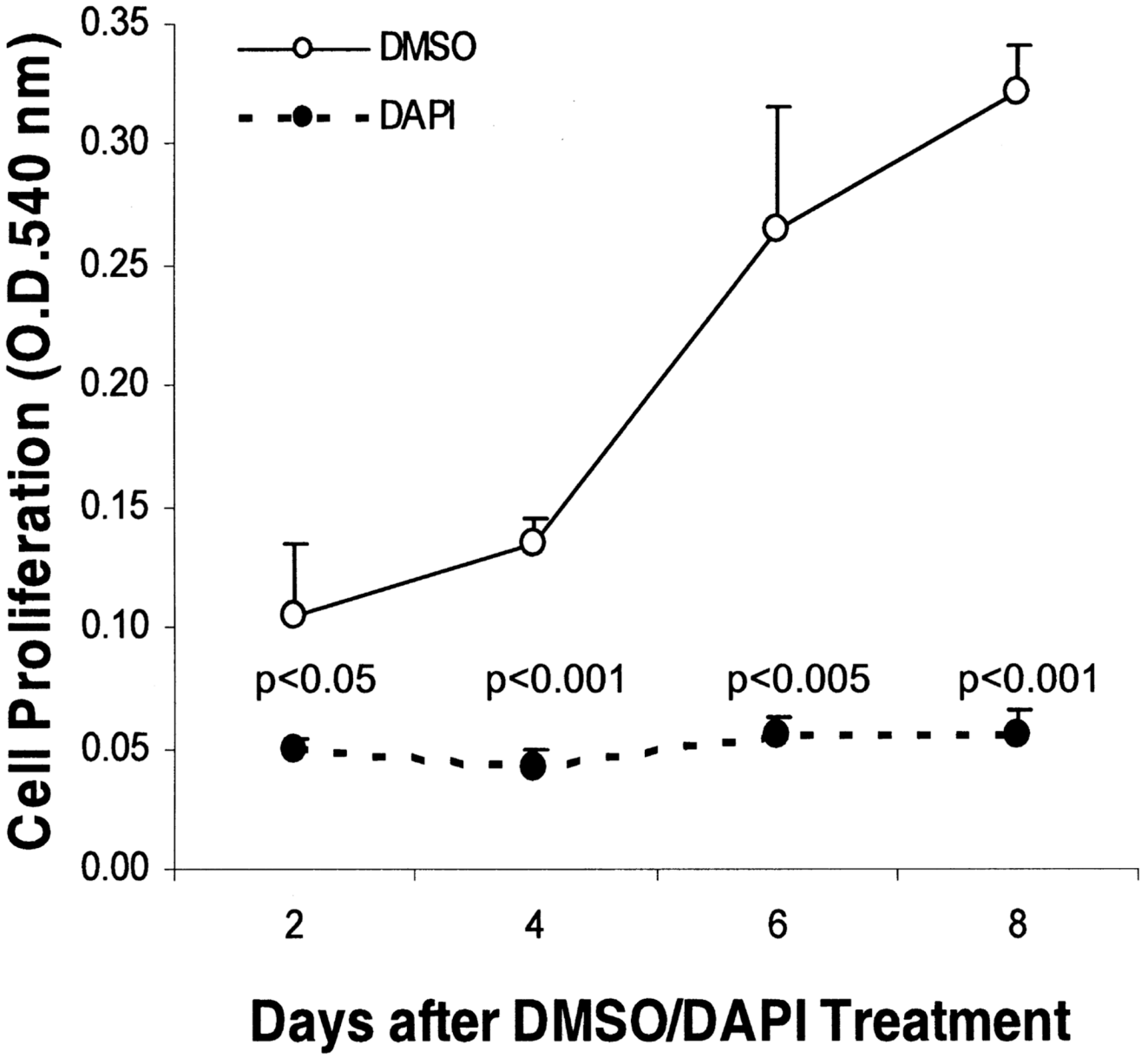

Figure 3.

DAPI labeling inhibits MSC proliferation. MSCs plated in triplicate on 24-well plates were treated with DAPI or DMSO overnight followed by washing and refeeding with the growth medium (day 0). MTT assays were performed at the time points indicated and cell proliferation was measured by $OD_{540\ nm}$. MSCs treated with DMSO or DAPI were statistically compared at each time point, and *p*-values are shown on the graph. Results are representative of two separate experiments, and are means ± SEs.

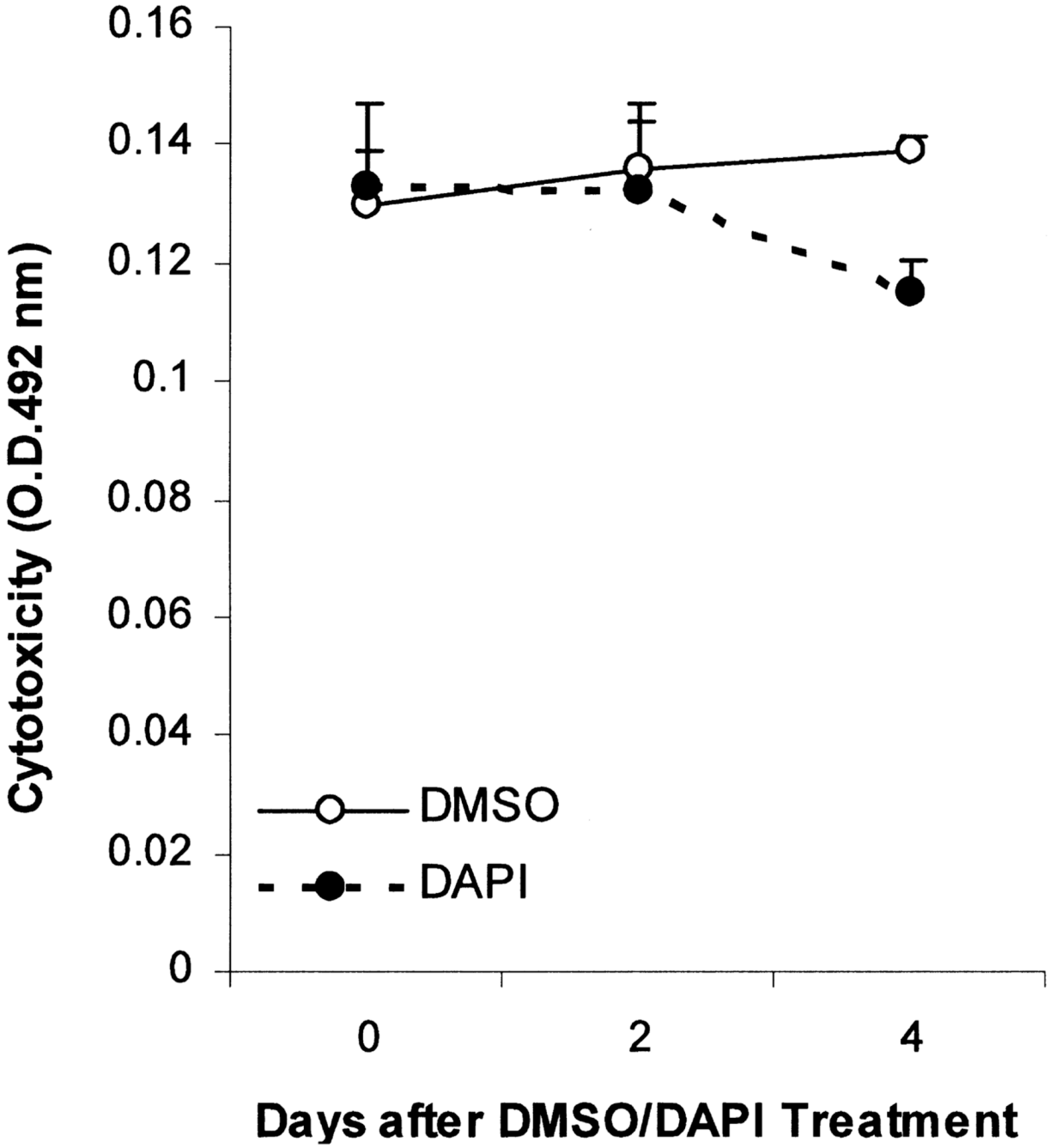

Figure 4.

DAPI-labeled MSCs retain full viability. MSCs were plated as described in Figure 3. Medium samples were removed from the wells at the time points indicated, and used for lactate dehydrogenase assays. Increases in $OD_{492\ nm}$ indicate cell injury or loss of cell membrane integrity. MSCs treated with DMSO or DAPI were statistically compared at each time point, and *p*-values are shown on the graph. Results are representatives of two separate experiments, and are means ± SEs.

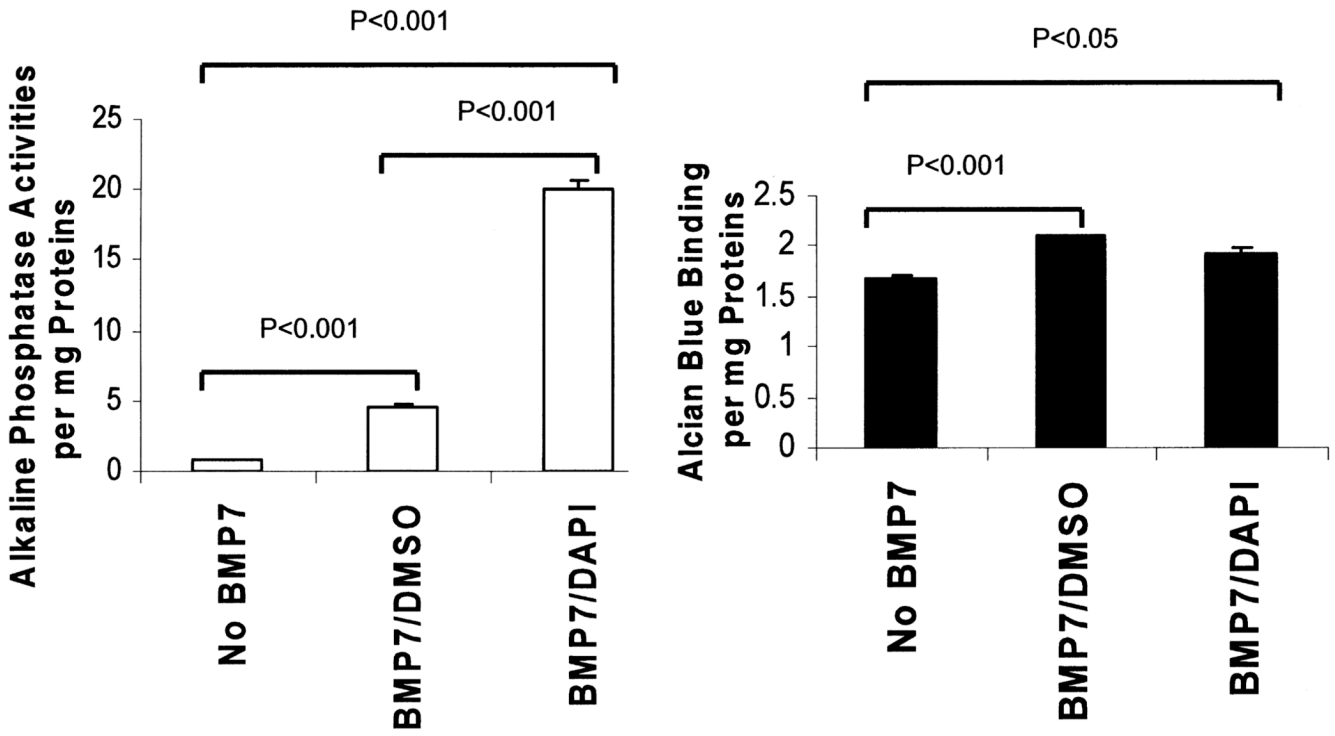

Figure 5.

DAPI labeling promotes BMP7-mediated MSC osteogenic differentiation in culture. MSCs for each group were plated in triplicate on 60-mm dishes. DMSO- and DAPI-treated cells were incubated with BMP7 for osteochondrogenic induction. Protein lysates were prepared and assayed for ALP activities (left panel for osteogenesis) and Alcian blue binding (right panel for chondrogenesis). Activities shown are expressed per milligram proteins. Results are representatives of two separate experiments, and are means ± SEs. Group comparisons are indicated by *p*-values above the bars.

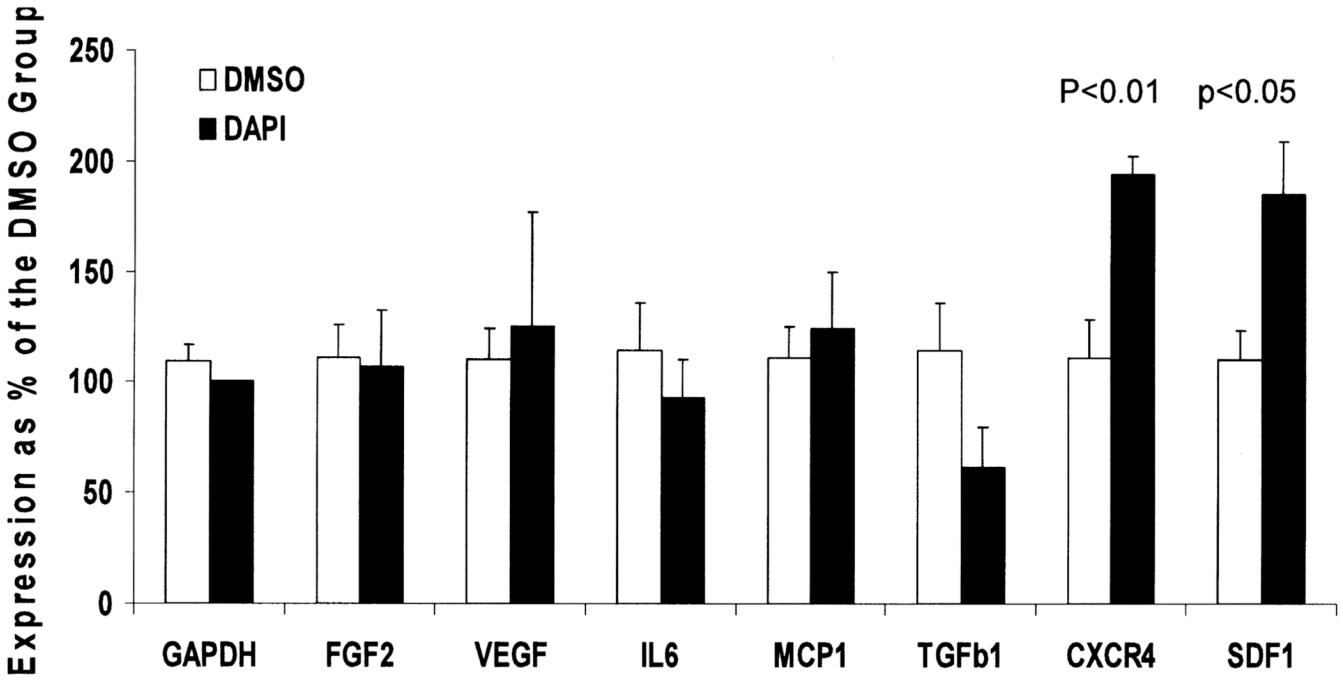

Figure 6.

DAPI labeling increases expression of the CXCR4 and SDF1 genes. MSCs were plated in triplicate for each group. RNA were isolated following the treatment, and analyzed by qRT-PCR using GAPDH as the reference gene. Results are representatives of four separate analyses, and are means ± SEs. No statistically significant differences between the DMSO and DAPI groups were found except for the CXCR4 and the SDF1 genes.

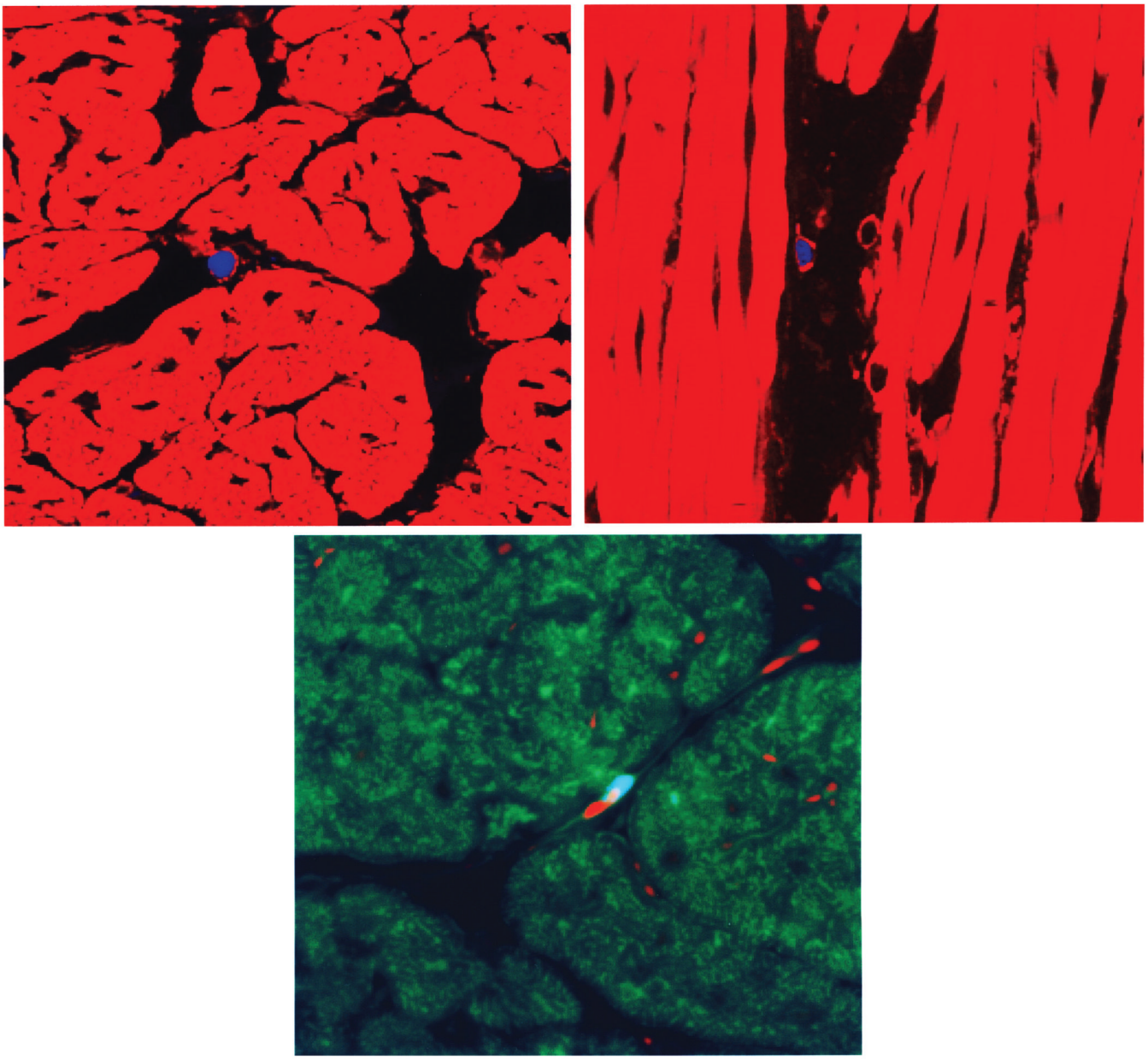

Figure 7.
Identification of DAPI-labeled MSCs after intracoronary infusion. Heart tissue samples were prepared 2 weeks after cell implantation by cryostat sectioning and counter-stained with TRITC-conjugated phalloidin (A and B) or with FITC-conjugated phalloidin and propidium iodide (C). Note the interstitial positions of the blue MSC nuclei in (A) and (B). Note the blue MSC nucleus positioned in line with propidium iodide-stained resident endothelial nuclei along the capillary structure in (C). The 400× *z*-stack images were obtained using an epifluorescent microscope Zeiss Axioimager Z1 with Apotome.